SPECIAL TOPIC — Optical field manipulation

Visible-light all-fiber vortex lasers based on mode selective couplers*

Chuchu Dong(董楚楚)[1], Jinhai Zou(邹金海)[1], Hongjian Wang(王鸿健)[1], Han Yao(尧涵)[2], Xianglong Zeng(曾祥龙)[2,†], Yikun Bu(卜轶坤)[1,‡], and Zhengqian Luo(罗正钱)[1,§]

[1] *Department of Electronic Engineering, Xiamen University, Xiamen* 361005, *China*

[2] *The Key Laboratory of Specialty Fiber Optics and Optical Access Network, Shanghai University, Shanghai* 200444, *China*

(Received 20 March 2020; revised manuscript received 11 June 2020; accepted manuscript online 3 July 2020)

We demonstrate visible-light all-fiber vortex lasers by incorporating the home-made mode selective couplers (MSCs). The MSC at green or red wavebands is fabricated by specially designing and fusing a single-mode fiber (SMF) and a few-mode fiber (FMF). The MSCs inserted into visible fiber cavities act as power splitters and mode converters from the LP_{01} to LP_{11} mode at green and red wavelengths, respectively. The red-light all-fiber vortex laser is formed by a 10-cm Pr^{3+}/Yb^{3+}:ZBLAN fiber, a fiber Bragg grating, a fiber end-facet mirror and the MSC at 635 nm, which generates vortex beams with $OAM_{\pm1}$ at 634.4 nm and an output power of 13 mW. The green-light all-fiber vortex laser consists of a 12-cm Ho^{3+}:ZBLAN fiber, two fiber pigtail mirrors, and the MSC at 550 nm, which generates vortex beams with $OAM_{\pm1}$ at 548.9 nm and an output power of 3 mW.

Keywords: fiber laser, vortex laser, mode selective coupler, visible-light

PACS: 42.55.Wd, 47.32.–y **DOI:** 10.1088/1674-1056/aba278

1. Introduction

Optical vortices are the light beams with helical phase wave-front distribution and orbital angular momentum (OAM). They have a phase singularity and carry different topological charges, so their light intensity distribution has the shape of a doughnut.[1–3] Because of these features in angular momentum and dynamic behavior, they are widely applied to optical tweezers,[4] high-resolution imaging,[5] particle trapping,[6] material processing,[7] and quantum information.[8] Currently, the methods of generating optical vortices in the free space mainly include, like spiral phase plates,[9] spatial light modulators,[10] cylindrical lens pairs,[11,12] Q-plates,[13] off-axis pumping,[14] and so on. However, the optical vortices produced by the above-mentioned methods have many limitations: (i) low purity of vortex beams and conversion efficiency, (ii) complex and bulky structure, (iii) high cost, and (iv) precise alignment of free-space optics with environment sensitivity. Compared with solid-state lasers, fiber lasers have drawn much attention for their unique advantages, such as compactness, low cost, ease of use, maintenance-free operation.[15–22] Many researchers attempted to generate optical vortices directly from fiber lasers. For example, Sun *et al.* used a specific fiber Bragg grating[23] and Wang *et al.* used a fiber mode-selective coupler (MSC)[24] to generate cylindrical vector or vortex beams.[25,26] However, all of them operated around 1 μm–2 μm near-infrared spectral region, in the visible spectral region (380 nm–760 nm), visible vortex fiber laser has not been fully exploited yet. In fact, visible vortex lasers have various applications to visible-light communications,[27–29] super-resolution imaging,[30] and micro-fabrication.[31] The main difficulties of realizing visible-light all-fiber lasers are: i) Although rare-earth-doped fluoride fibers as visible gain medium have low quantum energy and low background loss, they are difficult to fusion splice with other fibers, which increases the difficulty to construct visible all-fiber cavity; ii) The vortex devices operating in the visible region are relatively absent.

Most recently our research group reported visible-light all-fiber vortex lasers where directly generate visible vortex beam oscillations through the lateral offset splicing method,[32,33] but the offset splicing introduces large loss due to the mismatched mode fields. An alternative solution is to fuse an MSC into the visible fiber cavity, which can not only realize mode conversion from LP_{01} to LP_{11} mode, but also extract out the intracavity laser as laser output. Moreover, MSCs also have high conversion efficiency and vortex purity. Therefore, it is promising to explore the compact all-fiber visible

*Project supported by the National Natural Science Foundation of China (Grant Nos. 91750115 and 91750108), the Equipment Pre-research Project of Equipment Development Department of Central Military Commission, China (Grant No. 61404140112), and the Science and Technology Planning Project of Xiamen City, China (Grant No. 3502Z20183003).

†Corresponding author. E-mail: zenglong@shu.edu.cn

‡Corresponding author. E-mail: buyikun0522@xmu.edu.cn

§Corresponding author. E-mail: zqluo@xmu.edu.cn

vortex lasers by incorporating visible-wavelength MSCs.

In this paper, we designed and fabricated visible-wavelength MSCs at first, and then inserted them into red/green all-fiber laser cavities, respectively. We have achieved the all-fiber visible vortex laser generation at 548.9 nm and 634.4 nm. This is, to the best of our knowledge, the first demonstration of visible-light all-fiber vortex lasers based on MSCs, which has high purity and compact structure.

2. Visible-wavelength all-fiber mode selective couplers

The operation principle of visible MSCs is that the fundamental and higher-order modes are phase-matched, the SMF and the FMF change the transmitted energy according to the phase-matched conditions. The power of LP_{01} mode can be converted into a certain higher-order mode, when the length of the coupling region is equal to the periodic value. The SMF is pre-tapered to a specific diameter so that the propagation constant of the fundamental mode matches the one of the higher-order modes in the FMF. When the two propagation constants are equal, it is ideally phase-matched. In this experiment, The SMF is pre-tapered to some optimal diameters before fusing together with the FMF due to the asymmetrical fiber profile. The MSC consists of a single-mode fiber (SMF, HP650) and a few-mode fiber (FMF, core/cladding diameter = 10 μm/125 μm, NA = 0.23). We find, when the SMF diameters are around 110 μm and 112 μm for 638-nm and 520-nm MSCs, respectively, high-order mode (LP_{11}) conversion can be achieved, and the coupling efficiencies are up to 94% and 95% with insertion loss of about 0.5 dB and 0.3 dB. Then, a fiber coupler made up of two parallel fibers wounded, stretched, and fused together by hydrogen and oxygen flames, making their cores very close to each other. During the fusing process, the visible-light laser is input into the SMF port, and the power meter is used to monitor the output power ratio. When the ideal coupling ratio is reached, the fully self-motion fusing process is ceased. Finally, the fused coupler is packaged with a heat shrinkable tube. MSCs can not only realize the efficient conversion of LP_{01} to LP_{11}, but also act as power splitters that laser power is also reallocated in the coupling area.

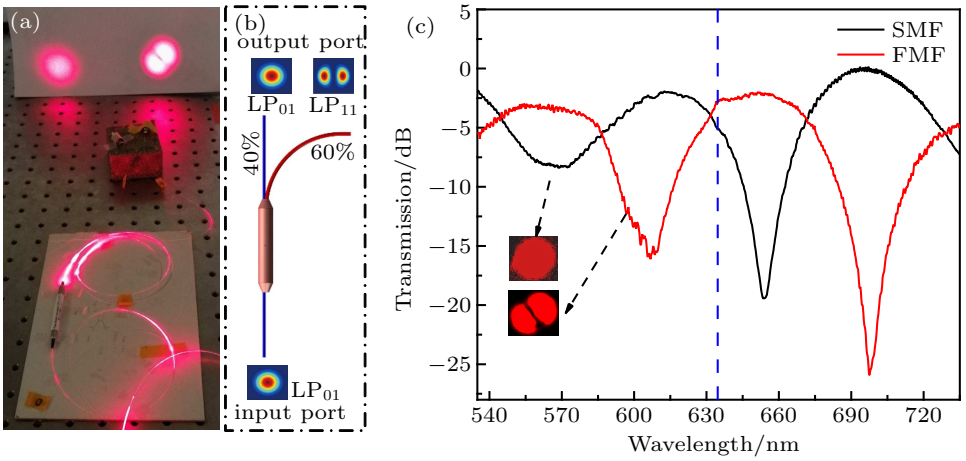

Fig. 1. (a) Photograph and (b) schematic diagram of the red-light MSC. (c) Transmission spectra of the red-light MSC, the inset shows the LP_{01} and LP_{11} modes.

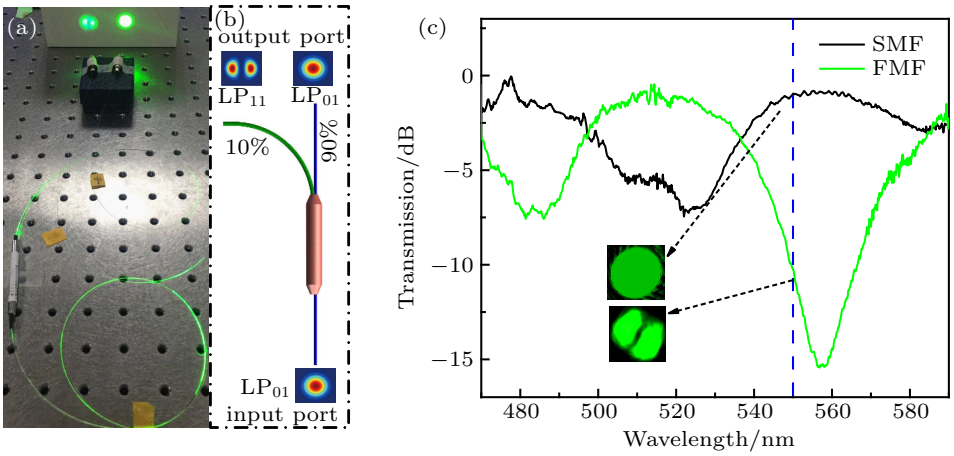

Fig. 2. (a) Photograph and (b) schematic diagram of the green-light MSC. (c) Transmission spectra of the green-light MSC, the inset shows the mode patterns of the LP_{01} and LP_{11} modes.

After the fabrication and package, we tested the performance of the visible-wavelength MSCs. As given in Fig. 1(a), when a red laser diode (LD) around 635 nm is poured into the SMF import, it is clearly seen that the SMF output port still output LP_{01} mode, and the FMF output port shows the strong LP_{11} mode. The output power ratio of the LP_{01} and LP_{11} modes measured by power meter is $\sim 40:60$ at 635 nm (Fig. 1(b)). Moreover, the transmission spectra of the LP_{01} and LP_{11} modes are further measured in Fig. 1(c), indicating that the MSC can work in a wide visible spectral range. In particular, the measured MSC insert loss is 0.8 dB at 635 nm. The green-light MSC is also measured by the similar methods. As shown in Fig. 2, the mode conversion from LP_{01} (SMF) to LP_{11} (FMF) mode can be clearly observed, and the output power ratio of the LP_{01} and LP_{11} modes is 90 : 10 at 550 nm. The broadband transmission spectra of the LP_{01} and LP_{11} modes in Fig. 2(c), which show the MSC enabling in the wide green waveband, the measured insertion loss is 0.7 dB at 550 nm.

3. Results and discussion

3.1. The 635-nm red-light all-fiber vortex laser based on MSC

Figure 3(a) gives the photograph of the red-light Pr^{3+}/Yb^{3+}:ZBLAN all-fiber vortex laser, and the schematic diagram is given in Fig. 3(b).

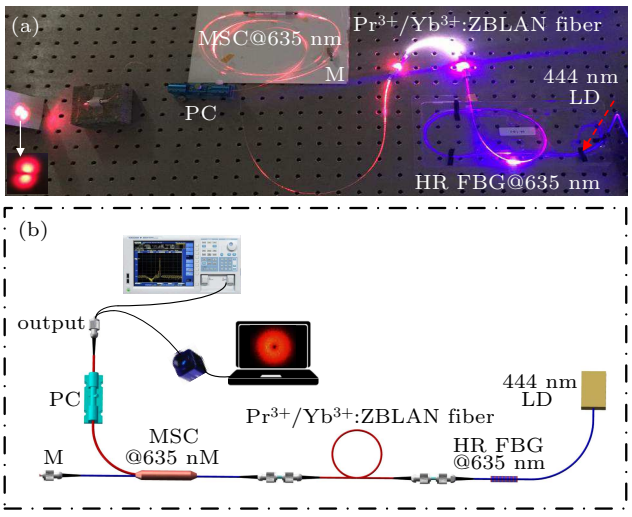

Fig. 3. (a) Photograph and (b) schematic diagram of the 635-nm red-light all-fiber vortex laser.

The red fiber vortex laser composes of a 444-nm fiber-coupled LD, a 10-cm Pr^{3+}/Yb^{3+}:ZBLAN fiber, a 98% high reflectivity fiber Bragg grating (FBG) at 635 nm, a fiber pigtail mirror M, an as-fabricated red-light MSC, and an in-line fiber polarization controller (PC). The Pr^{3+}/Yb^{3+}:ZBLAN fiber as a down-conversion visible gain medium has a Pr^{3+} concentration of 3000 ppm and an Yb^{3+} concentration of 20000 ppm, and its core diameter and numerical aperture are 2.8 μm and 0.23, respectively. The fluoride fiber and two silicate fiber are butt-coupling by ceramic sleeves to achieve high coupling efficiency ($\sim 85\%$). The resonator is made up of the 635-nm highly-reflective FBG and the home-made fiber end-facet mirror M. A plasma sputter deposition technology is used to fabricate fiber end-facet mirror by coating SiO_2/Ta_2O_5 dielectric films onto the facet ends. The mirror M is highly reflective at 635 nm, and a reflectivity is 99%. All the other fibers in the cavity are Nufern 780 HP. The MSC was inserted in the cavity to excite the LP_{11} mode (including four vector modes) into FMF, which could further enable vortex laser with high purity to be realized. The role of the in-line PC at the output port is to make the phase difference between the two vector modes up to $\pi/2$ to further obtain the donut-shaped beam.

In our experiment, red-light laser was generated when pump power increased to 36.3 mW. We used a spectrograph to measure the output laser spectrum (see Fig. 4). A central wavelength of 634.4 nm was measured at the pump power of 52.3 mW in the red-light laser, and the linewidth of 3 dB is 0.4 nm. And we found that the central wavelength stays the same as the pump power increases.

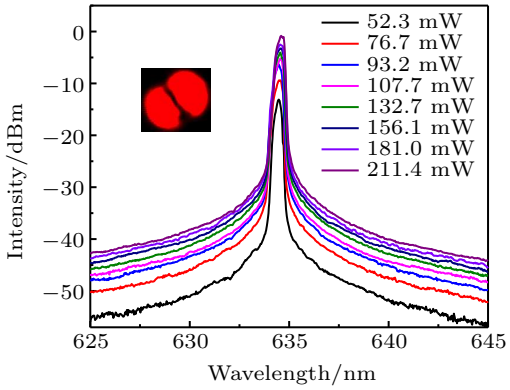

Fig. 4. Optical spectra of the 635-nm red-light laser at different powers.

We also further investigated the mode characteristics of the output red laser. The near-field intensity distributions of 634.4-nm laser are shown in Figs. 5(a) and 5(b), and the two-lobe-shaped beams are typically vector modes of the LP_{11}. Technically, LP_{11} mode can be superimposed by four vector modes (*i.e.*, TE_{01}, TM_{01}, HE_{21}^{even}, and HE_{21}^{odd}), and their combination corresponds to LP_{11}^{even} and LP_{11}^{odd}.[34] By adjusting the PC, the parameters (*e.g.*, birefringence) of the FMF are changed by the stress, resulting in the two modes with different phase velocities. By adjusting the stress in the PC, the phase difference of the two orthogonal modes reaches $\pi/2$. Thus, ± 1-order OAM beams with symmetrical annular intensity distribution and helical phase front could be obtained.[35,36] Figures 5(c) and 5(d) give the corresponding donut-shaped patterns by properly adjusting the PC at the output. Figures 5(e) and 5(f) depict the counterclockwise and clockwise interference patterns of the donut-shaped beams, indicating that the

obtained vortex beams with $OAM_{\pm1}$ in the red-light fiber laser. By tight bend approach,[23] we measured the purity of the 635-nm vortex beams with $OAM_{\pm1}$ is 91.4% and 92.8%. We also measured the effect of pump power on output power in the red-light vortex laser.

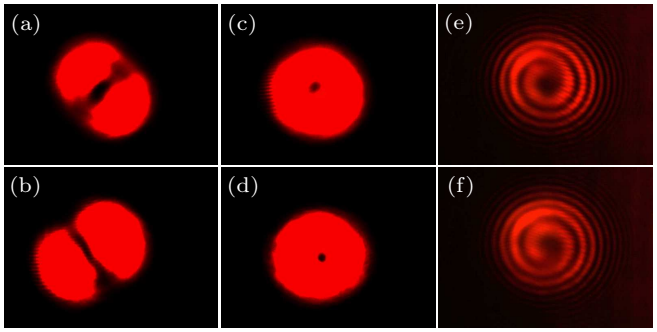

Fig. 5. Near-field intensity distributions of the LP_{11} mode in the red-light all-fiber laser. (a) and (b) Intensity patterns of the LP_{11} mode. (c) and (d) Intensity profiles of donut-shaped patterns. (e) and (f) Counterclockwise and clockwise spiral interferograms.

Figure 6 shows the output power up to 13 mW, and the output power increases linearly with the pump power. In addition, we observed that the profile and intensity of LP_{11} mode field remain constant for a long time under the same state, indicating that the vortex mode has a certain stability.

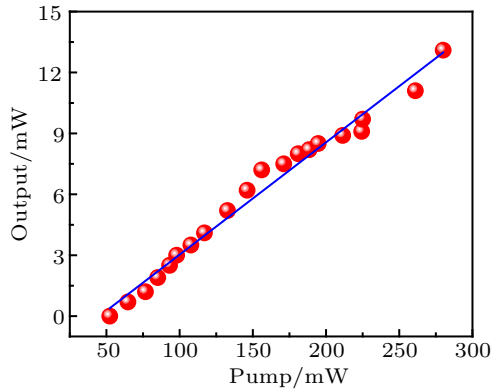

Fig. 6. The power of the red vortex laser under different pump powers.

3.2. The 550-nm green-light all-fiber vortex laser based on MSC

Figures 7(a) and 7(b) show the photograph and schematic diagram of the green-light all-fiber vortex laser. A 444-nm fiber-coupled LD plays an important role as the pump source, and a 12-cm Ho^{3+}:ZBLAN fiber with a concentration of 1000 ppm is used as gain medium to provide green-light gain. Its core diameter and numerical aperture are 8.4 μm and 0.16. The Ho^{3+}:ZBLAN fiber and silicate fiber are efficiently coupled by two ceramic sleeves. The linear resonator consists of two homemade fiber pigtail mirrors (M1 and M2). As given in Fig. 7(b), the M1 and M2 are carefully designed, they are highly reflective at 550 nm, with reflectance of 99.6% and 94.6%, respectively. It is worth noting that the M1 has high transmissivity of 85% at 444 nm so that the pump laser can mostly inject into the cavity through the fiber mirror M1. The MSC acts as a high-order mode transformer as well as an output splitter.

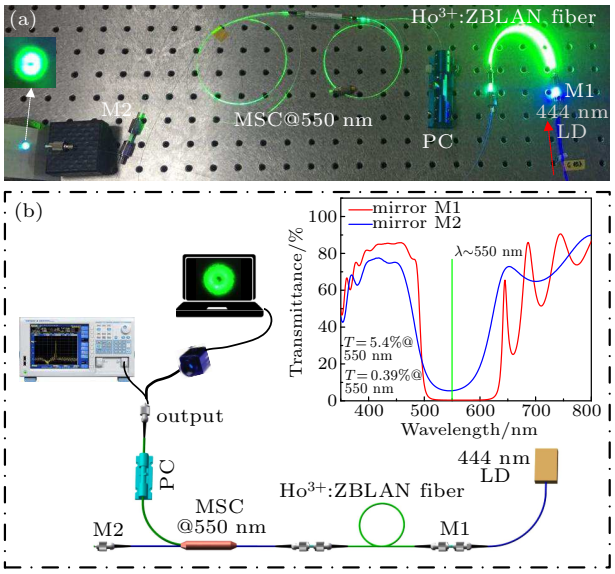

Fig. 7. (a) Photograph and (b) schematic diagram of the 550-nm green-light all-fiber vortex laser.

The 550-nm laser has a threshold of 373 mW. Figure 8 shows the output optical spectra of the 550-nm laser. The central wavelength was measured to be 548.9 nm, and the linewidth of 3 dB is 0.4 nm. We measured the spectra at different powers, and found that an increasing of pump power does not change the central wavelength.

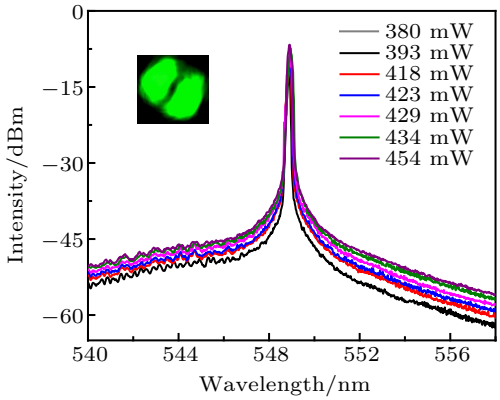

Fig. 8. Optical spectra of the 550-nm green-light laser at different powers.

Subsequently, we observed the characteristics of the azimuthally/radially polarized beams in the green-light laser by a visible CCD. Figures 9(a) and 9(f) shows donut-shape intensity profiles, to verify whether they are azimuthally or radially polarized beams, we insert a polarizer in front of the CCD to observe property of the vortex beams. By rotating the polarized axis direction of the polarizer, two-lobe-shaped intensity patterns are obtained. Figures 9(b)–9(e) show near-field intensity patterns through the polarizer. It can be seen that the orientations of intensity patterns are perpendicular to the polarized axis of the polarizer, indicating that the cylindrical vector

beam is azimuthally polarized as TE_{01} mode. Figures 9(g)–9(j) show the intensity patterns are the same direction as the polarized axis of the polarizer, indicating that the cylindrical vector beam is radially polarized as TM_{01} mode. In particular, OAM modes also can be obtained by compressing and rotating of the PC. The typical near-field profiles (two-lobe) of the LP_{11} mode can be seen in Figs. 10(a) and 10(b). Figures 10(c) and 10(d) show the donut-shaped intensity profiles, and we further measured their spiral interferometry patterns as seen in Figs. 10(e) and 10(f). The results indicated that green-light vortex beams with $OAM_{\pm1}$ were successfully generated. Finally, we explored the effect of pump power on output power in green-light vortex lasers. Figure 11 shows that the average power of the output laser increases linearly with the pump power, and a maximum power of 3 mW was obtained. The purity of the 550-nm vortex beams with $OAM_{\pm1}$ is 88.4% and 90.7%, and the profile and intensity of the LP_{11} mode field can keep stable for a long time under the same state.

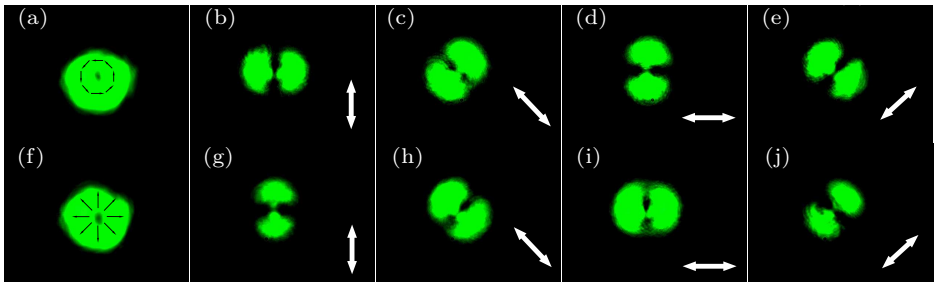

Fig. 9. Near-field distributions of azimuthally/radially polarized beams in the green-light all-fiber laser. (a) and (f) Donut-shape intensity profiles. (b)–(e) and (g)–(j) Near-field intensity patterns with rotation of a polarizer.

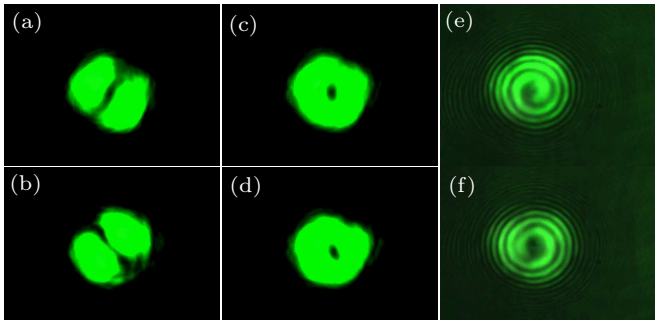

Fig. 10. Near-field intensity distributions of the LP_{11} mode in the green-light all-fiber laser. (a) and (b) Intensity patterns of the LP_{11} mode. (c) and (d) Intensity profiles of donut-shaped patterns. (e) and (f) Counterclockwise and clockwise spiral interferograms.

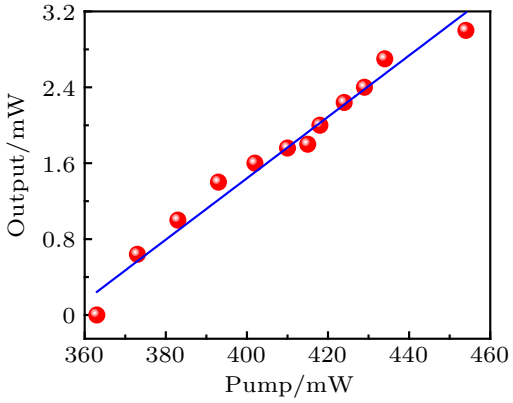

Fig. 11. The power of the green vortex laser under different pump powers.

4. Conclusion

In summary, visible-light all-fiber vortex lasers based on MSCs have been proposed and demonstrated. The MSCs operating in the red and green wavebands were fabricated and characterized. Combining the MSCs and the fiber pigtail mirrors to constitute the all-fiber visible cavities, we successfully achieved the green/red vortex fiber lasers at 548.9 nm and 634.4 nm. The red vortex laser generates the ±1 order OAM and the output power of 13 mW, and the green vortex laser also generates the ±1 order OAM and the output power of 3 mW. The purity of vortex lasers is high, but because the length of ZBLAN fiber are not optimized and the MSCs have slightly larger loss, the laser conversion efficiency and the output power are not optimal. In the follow-up experiments, we will optimize the length of the ZBLAN fiber and the insertion loss of MSCs to improve the efficiency and try to propose visible-light pulse vortex lasers.

References

[1] Yao A M and Padgett M J 2011 *Adv. Opt. Photon.* **3** 161
[2] Allen L, Beijersbergen M W, Spreeuw R J and Woerdman J P 1992 *Phys. Rev. A* **45** 8185
[3] Allen L, Padgett M J and Babiker M 1999 *Prog. Opt.* **39** 291
[4] Padgett M and Bowman R 2011 *Nat. Photon.* **5** 343
[5] Xie X, Chen Y, Yang K and Zhou J 2014 *Phys. Rev. Lett.* **113** 263901
[6] Kawauchi H, Yonezawa K, Kozawa Y and Sato S 2007 *Opt. Lett.* **32** 1839
[7] Hnatovsky C, Shvedov V G, Krolikowski W and Rode A V 2010 *Opt. Lett.* **35** 3417
[8] Wang X L, Cai X D, Su Z E, Chen M C, Wu D, Li L, Liu N L, Lu C Y and Pan J W 2015 *Nature* **518** 516
[9] Schemmel P, Pisano G and Maffei B 2014 *Opt. Express* **22** 14712
[10] Ostrovsky A S, Rickenstorff-Parrao C and Arrizón V 2013 *Opt. Lett.* **38** 534
[11] Beijersbergen M W, Allen L, van der Veen H E L O and Woerdman J P 1993 *Opt. Commun.* **96** 123
[12] Li N, Xu B, Cui S, Qiu X, Luo Z, Xu H, Cai Z, Chen L and Moncorge R 2019 *IEEE Photon. Technol. Lett.* **31** 1457
[13] Gregg P, Mirhosseini M, Rubano A, Marrucci L, Karimi E, Boyd R W and Ramachandran S 2015 *Opt. Lett.* **40** 1729
[14] Ma Y, Valles A, Tung J C, Chen Y F, Miyamoto K and Omatsu T 2019 *Opt. Express* **27** 18190

[15] Wang H, Zou J, Dong C, Du T, Xu B, Xu H, Cai Z and Luo Z 2019 *Opt. Lett.* **44** 4423
[16] Du T, Luo Z, Yang R, Huang Y, Ruan Q, Cai Z and Xu H 2017 *Opt. Lett.* **42** 462
[17] Jackson S D 2012 *Nat. Photon.* **6** 423
[18] Renninger W H, Chong A and Wise F W 2008 *Phys. Rev. A* **77** 023814
[19] Luo Z C, Liu M, Liu H, Zheng X W, Luo A P, Zhao C J, Zhang H, Wen S C and Xu W C 2013 *Opt. Lett.* **38** 5212
[20] Kieu K, Renninger W H, Chong A and Wise F W 2009 *Opt. Lett.* **34** 593
[21] Chernikov S V, Zhu Y, Taylor J R and Gapontsev V P 1997 *Opt. Lett.* **22** 298
[22] Martinez A and Sun Z 2013 *Nat. Photon.* **7** 842
[23] Sun B, Wang A, Xu L, Gu C, Lin Z, Ming H and Zhan Q 2012 *Opt. Lett.* **37** 464
[24] Yan Y, Wang J, Zhang L, Yang J Y, Fazal I M, Ahmed N, Shamee B, Willner A E, Birnbaum K and Dolinar S 2011 *Opt. Lett.* **36** 4269
[25] Wang T, Wang F, Shi F, Pang F, Huang S, Wang T and Zeng X 2017 *J. Light. Technol.* **35** 2161
[26] Wang T, Shi F, Huang Y, Wen J, Luo Z, Pang F, Wang T and Zeng X 2018 *Opt. Express* **26** 11850
[27] Oubei H M, Li C, Park K H, Ng T K, Alouini M S and Ooi B S 2015 *Opt. Express* **23** 20743
[28] Chi Y C, Hsieh D H, Tsai C T, Chen H Y, Kuo H C and Lin G R 2015 *Opt. Express* **23** 13051
[29] Oubei H M, Duran J R, Janjua B, Wang H Y, Tsai C T, Chi Y C, Ng T K, Kuo H C, He J H, Alouini M S, Lin G R and Ooi B S 2015 *Opt. Express* **23** 23302
[30] Li Z, Zhang T, Wang Y Q, Kong W J, Zhang J, Huang Y J, Wang C T, Li X, Pu M B and Luo X G 2018 *Laser Photon. Rev.* **12** 1800064
[31] Di S and Jin J 2019 *Int. J. Optomechatronics* **13** 30
[32] Zou J, Wang H, Li W, Du T, Xu B, Chen N, Cai Z and Luo Z 2019 *IEEE Photon. Technol. Lett.* **31** 1487
[33] Zou J, Kang Z, Wang R, Wang H, Liu J, Dong C, Jiang X, Xu B, Cai Z, Qin G, Zhang H and Luo Z 2019 *Nanoscale* **11** 15991
[34] Zhang W, Wei K, Huang L, Mao D, Jiang B, Gao F, Zhang G, Mei T and Zhao J 2016 *Opt. Express* **24** 19278
[35] Lu J, Meng L, Shi F, Liu X, Luo Z, Yan P, Huang L, Pang F, Wang T, Zeng X and Zhou P 2018 *Opt. Lett.* **43** 5841
[36] Wang T, Wang F, Shi F, Pang F, Huang S, Wang T and Zeng X 2017 *Optical Fiber Communication Conference*, March 19–23, 2017, Los Angeles, California, USA, p. Tu3J.2